Research papers

Desiccation of the Transboundary Hamun Lakes: Natural or Anthropogenic?

Mahdi Akbari[a,*], Ali Mirchi[b], Amin Roozbahani[c], Abror Gafurov[d], Bjørn Kløve[a] and Ali Torabi Haghighi[a]

a Water, Energy and Environmental Engineering Research Unit, Faculty of Technology, University of Oulu, Finland

b Department of Biosystems and Agricultural Engineering Oklahoma State University, Stillwater, USA

c Nimab-tose Consulting Engineering Company, Tehran, Iran

d GFZ German Research Centre for Geosciences, Section 5.4 Hydrology, Potsdam, Germany

**Corresponding author: mahdi.akbari@oulu.fi*

The paper is a non-peer reviewed preprint submitted to EarthArXiv. Also, this manuscript has been submitted in **Great Lake Research Journal** for peer review. Please feel free to contact corresponding author for any question or feedback.

Abstract

This paper investigates the hydrologic and water management reasons behind the desiccation of the Hamun Lakes in the Iran-Afghanistan border region. We analysed changes in Hirmand (or Helmand) River flow, the main tributary providing 70% of the lakes' total inflow, and precipitation during 1960-2016 by calculating standardized indices for precipitation (SPI) and discharge (SDI). Also, we applied Normalized Difference Spectral Indices (NDSIs) using satellite images from 1987 to present to observe monthly areal change of the lakes. The transboundary water body is responding to changes in regional water management, which has severely reduced the lakes' inflow. Upstream water regulation in Afghanistan coupled with reservoir construction on the Iranian side has caused nearly full desiccation of major parts of the lake system. There is a discernible shift in the relation between the Hirmand River flow at the international border and upstream precipitation over the lakes' basin before and after 2004. From 1960 to 2003, high river flows were expected to feed the lakes due to high precipitation over the basin. However, the Hirmand River flow at the border declined after 2004 despite large amounts of upstream precipitation, including the largest recorded amounts, especially in the Hindu Kush mountains. Further, environmental water stress caused by anthropocentric water management in Iran by reservoir construction has impacted the area of the lakes. Although a long period of drought from 1998-2004, i.e. climatic driver, decreased the lakes' area, the lake system is primarily falling victim to anthropogenic flow alterations in the transboundary river basin. The lakes' shrinkage places socio-economic stress on an already-vulnerable region with important public health implications as the exposed lake beds turn into major sources of sand and dust storms.

Key words

Standardized Precipitation Index (SPI), Standardized Discharge Index (SDI), Normalized Difference Spectral Indices (NDSIs), Water Management, Lake Desiccation, Iran-Afghanistan Border Region

36 **Graphical abstract**

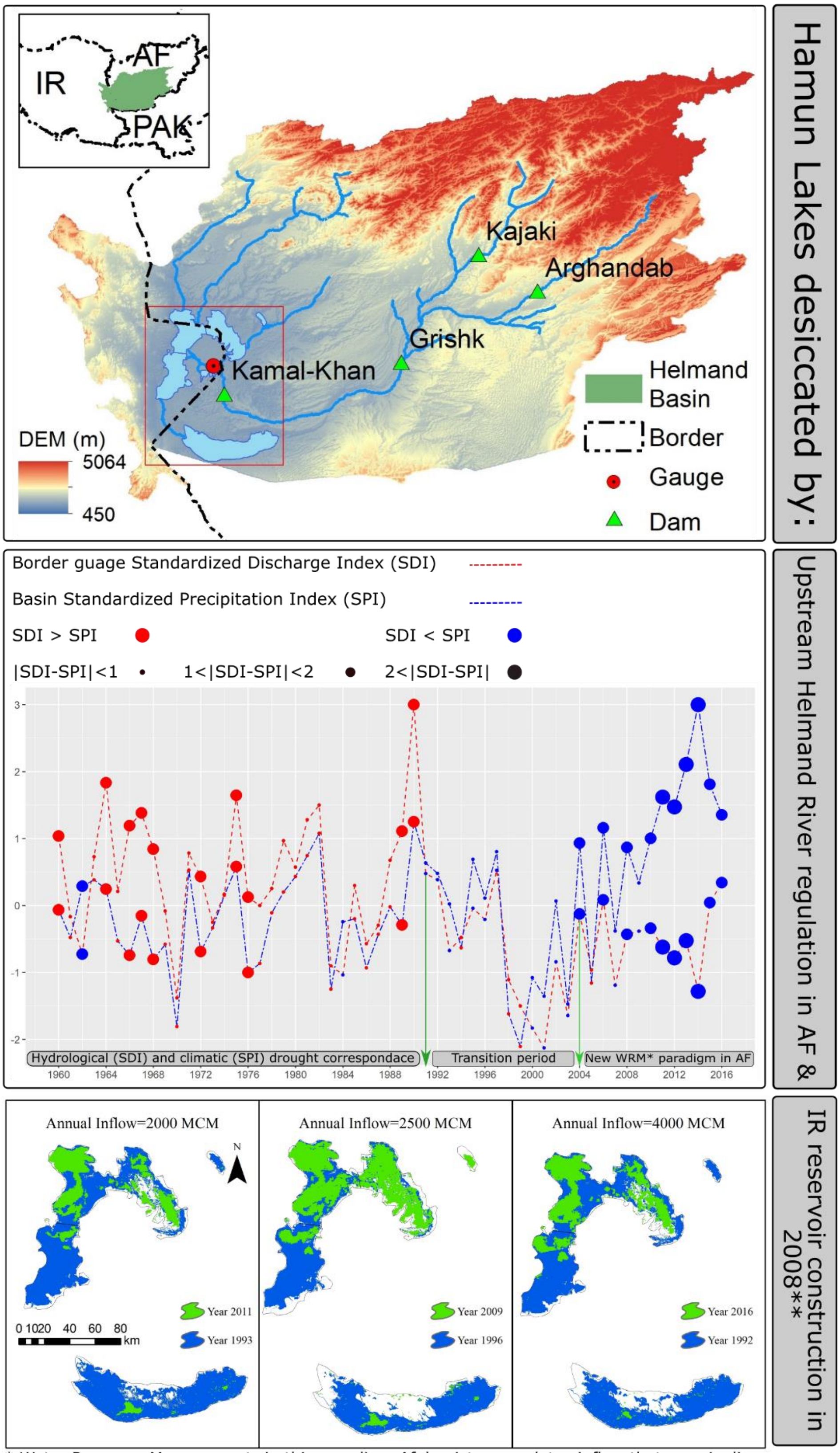

* Water Resource Management: in this paradigm Afghanistan regulates inflow that marginalizes environmental flow to the Hamun lakes.

** After 2008, Iran has constructed a reservoire with more than 800 MCM capacity which has intensified desiccation process of the lakes.

37

1. Introduction

The Hamun Lakes, the largest (> 8000 km^2) fresh body of water in the Iran plateau comprised of four connected lakes, has nearly desiccated in recent years. Although climatic variation is an important driver of the change of water-land in large scales (Akbari et al., 2020; Ehsani et al., 2020; Haghighi and Kløve, 2015; Milly and Dunne, 2016; Rahimi et al., 2020), there is growing concern that human activities are a substantial, sometimes dominant reason for decline of shrinking water bodies which trigger a host of environmental and economic consequences (AghaKouchak et al., 2015; Chaudhari et al., 2018; Haghighi et al., 2020; Khazaei et al., 2019; Zaki et al., 2020). The dry-up of water bodies, i.e. so-called Aral Sea desiccation syndrome (AghaKouchak et al., 2015), has been observed in Central Asia (Micklin, 1988) and northwestern Iran (Akbari et al., 2019; Alborzi et al., 2018; Torabi Haghighi et al., 2018)

Hamun Lakes are located in the Iran-Afghanistan border zone in the Sistan region (Figure 1-a) within the transboundary Helmand Basin. The lake system is a Ramsar site (The Convention on Wetlands, 1975) that is crucial for the economy and environment (Rashki et al., 2012). The main rivers that sustain the lakes originate in Afghanistan. Hirmand (or Helmand) River, the most important river feeding the lake system and a crucial water source for Afghan and Iranian farmers (Ahlers et al., 2014), is shared based on the bilateral treaty of 1973. The treaty, known as the Water Protocol (WP), guarantees annual water delivery of 0.820 km^3 to Iran by Afghanistan (Iran Ministry of Enegry (MoE), 2013), providing a basis for monthly allocation of river flow between the two sovereign states (Figure 1-f). Agricultural development and water resources management in the region is giving rise to classic upstream-downstream water tensions that adversely affect the socio-economically vulnerable residents in the border region, including the Sistan and Baluchistan province of Iran (Ahlers et al., 2014).

The exposed bed of the Hamun Lakes are a major dust source in southwest Asia (Goudie and Middleton, 2006) due to strong winds known as “120-day wind” (Hossenzadeh, 1997). Theses winds are frequent and intensive, especially during the summer (Goudie and Middleton, 2000), and their speed is probable to reach over 100 km/s (Meteorological Department of Sistan and Baluchestan, 2020). The sand and dust storms affect the Sistan region in Iran, southwest Afghanistan, and Pakistan (Alam et al., 2011; Goudie and Middleton, 2000; Rashki et al., 2012). Zaranj City (Figure 1-b) is the largest population centre (~160,000 people) in Afghanistan close to the lakes (Afganistan Ministry of Urban Development Affairs, 2015). The population in urban areas is larger on the Iranian side where Zahedan (~590,000 people) and Zabol (~134,000 people) are located (Statistical Center of Iran, 2016). In 2011, the concentration of mean annual Particulate Matter with 10 and 2.5 micrometres or less in diameter (PM_{10} and $PM_{2.5}$) in the Zabol air reached 527 and 217 $\mu g/m^3$, respectively (WHO, 2016), far exceeding WHO’s safe concentration thresholds for PM_{10} (20 $\mu g/m^3$) and $PM_{2.5}$ (10 $\mu g/m^3$). Consequently, respiratory diseases are a common public health hazard in Zabol with medical costs exceeding USD 166.7 Million U.S. during 1999–2004 (Miri et al., 2007).

As mounting concerns about the drying of the Hamun Lakes give rise to potential water conflicts in this transboundary basin (Dehgan et al., 2014; Mianabadi et al., 2021), it is necessary to evaluate whether the shrinkage is governed by climatic conditions or if the problem has emerged as a result of anthropogenic water regulation. This understanding is an important precursor for effective plans to protect the socio-ecological system based on binational cooperation between Iran and Afghanistan. To this end, we investigate the climatic and hydrological drivers of the desiccation of the Hamun Lakes alongside a shift in water management paradigm that has marginalized environmental flows. Our analysis covers water resources management on both sides of the border, namely upstream dams in Afghanistan, as well as water regulation of the Hirmand River in Iran by constructing reservoirs in the Sistan region. We study hydrological and meteorological droughts in the Hirmand River sub-basin from 1960-2016 to characterize the Hirmand River flow alteration at the international border. The hydro-climatological investigation of the connected lake system's monthly areal trend from 1987 to 2020, reveals the mechanism of desiccation, which is essential for determining the reasons behind the decline of this complex water body with far-reaching socio-economic and environmental consequences.

2. Materials and Methods

2.1. Study area

Helmand Basin (area: ~350,000 km^2) is the largest basin in Afghanistan, covering over half of the country. Most of this transboundary basin (~87%) is located in Afghanistan, 9% in Iran and 4% in Pakistan (Figure 1-a). As the terminal point of an endorheic basin, the Hamun Lake system is primarily fed by rivers that originate in the Hindu Kush mountain range. Other major tributaries besides Hirmand (or Helmand) River (mean annual flow: ~ 6 km^3) include Farah, Khash and Adraskhan (or Harut) with a mean annual flow of about 1.3, 0.3 and 0.2 km^3, respectively (Williams-Sether, 2008) (more detail in Appendix A). Two of the largest dams in Afghanistan, namely Kajaki (2.5 km^3) and Arghandab (or Dahla) (0.5 km3), were built in this basin in 1952 (Lehner et al., 2011). The maximum monthly inflow to these dams occurs in April, averaging about 1.5 and 0.6 km^3, respectively (Williams-Sether, 2008). Also, the Kamal-Khan Dam current capacity is over 50 million cubic meters which is the largest hydraulic structure on the Hirmand River after the Kajaki Dam (Figure 1-a). Construction of this dam began in 1996 but was halted due to the civil war in Afghanistan. The project recommenced in 2011 and phase II was completed in 2015. Work on phase III began in 2017. The objective has been to provide water for irrigation of agricultural land in Afghanistan, flood protection, drinking water and generation of 9 MW of electricity. The target area after the Kamal-Khan Dam operation is irrigating 174,000 hectares (Mianabadi et al., 2021).

According to the Köppen-Geiger climate classification (Kottek et al., 2006), the Helmand Basin's climate varies from highlands to downstream areas, ranging from snow climate with dry summers (Ds) in the Hindu Kush mountain range to warm temperate climate with dry summer (Cs) in the foothills of the Hindu Kush mountains and steppe climate (BS) and desert climate (BW) downstream of Kajaki and Arghandab Dams (Appendix A, Figure S 1-a). Based on the Global Precipitation Climatology Centre (GPCC) dataset (Schneider et al., 2011), the basin's annual precipitation varies from more than 1200 mm in the Hindu Kush highlands to less than 60 mm in the lowlands near the Hamun Lakes (see Appendix B).

The Hamun Lakes consist of three connected Lakes above Shile Canal (Figure 1-b), namely Hamun-i Puzak ($max\ area = 1{,}500$ km^2), Hamun-i Sabari ($max\ area = 1{,}500$ km^2) and Hamun-i Hirmand ($max\ area = 2{,}000$ km^2), and a deeper terminal lake named Gaud-i Zirreh ($max\ area = 3{,}000$ km^2) (Figure 1-a). Hamun-i Puzak with entrance elevation of 480 meter (m) above mean sea level (AMSL) at the outlet of the Paryan River (Figure 1-c) is the first lake in this cascading lake system. The lowest bed elevation at Hamun-i Puzak is 475.5 m AMSL, and excess flow after filling this lake spills into Hamun-i Sabari at 477 meter AMSL, which discharges into the downstream Hamun-i Hirmand at 474.5 m AMSL (Figure 1-c). Finally, the last lake is Gaud-i Zirreh, which is fed by Shile Canal in the south of Hamun-i Hirmand (Figure 1-b). Mean depth and capacity of the first three lakes (Hamun-i Puzak, Hamun-i Sabari and Hamun-i Hirmand) is less than 2 meters and 3 km^3, respectively, while Gaud-i Zirreh is the deepest lake with a mean depth of 10 m. Mean annual flow for Shile Canal (inflow to Gaud-i Zirreh) at Pol-Shile station is about 3 km^3 (1990-1998), which decreased to almost zero after 1999 (Hamoon International Wetland Research Institute of Zabol University (HIWRI), 2017).

Hirmand River bifurcates into two rivers after entering Iran: Sistan and Paryan Rivers (Figure 1-d). Paryan River flows to Hamun-i Puzak, and Sistan River finally ends in Hamun-i Sabari and Hamun-i Hirmand (Figure 1-b). Some parts of the Sistan River flow were diverted by Kahak diversion dam (Figure 1-d) to four reservoirs named Chah Nimeh Reservoirs (CNR1 through 4) through the Feeder Canal (shown as FC in Figure 1-d with $capacity = 600\ m^3/sec$). CNR1 (Cap: 0.220 km^3), CNR2 (Cap: 0.090 km^3), and CNR3 (0.320 km^3) were constructed in 1983. The last and largest reservoir, i.e. CNR4 (Cap: 0.810 km^3) was commissioned in 2008 but initial filling began sooner (Absaran Consulting Company, 2015). The main purposes of CNRs in Iran are to meet agricultural (0.4 km^3/yr), domestic (0.11 km^3/yr), and industrial (0.03 km^3/yr) demands of the Sistan region, totalling 0.54 km^3/yr (MoE, 2014). CNRs are connected, each spilling to the next at 480 m AMSL. Feeder Canal discharges into CNR1, and then into CNR2 until all CNRs are sequentially filled. When all CNRs are full, the overflow is directed to the Sistan River from the north of CNR1 and west of CNR4 by two canals known as Head Race (HR shown in Figure 1-d). Both HRs have been equipped with floodgate to regulate outflow. The evaporation rate near CNRs is 2,495 mm/yr and the annual volume of evaporation from the CNRs is 0.306 km^3 (MoE, 2014).

2.2. Data

The spatiotemporal scope of the study was determined based on data availability and predominant inflow into the lakes. We limited our investigation to Hirmand River sub-basin (Figure 1-a) for 1960-2016. The annual flow data from 1960 to 2016 for Choto and Kahak gauges on Sistan and Paryan Rivers next to the border on the Iranian side (Figure 1-d) were obtained from MoE (MoE, 2014). Also, USGS (Williams-Sether, 2008) data-base provides flow data for period 1955-1980 at gauges located in Afghanistan (Figure 1-a) . The magnitude of discharge into the lakes has significant uncertainty (MoE, 2015) due to lack of river flow data in Afghanistan after 1980 to quantify the exact contribution of Adraskan, Farah and Khash rivers (Figure 1-b), as well as missing water withdrawal data in mid-basin in Iran (from international border to the lakes). Approximately 70% of the flow into the Hamun Lakes is from Hirmand River while the rest is supplied mostly by Farah River based on USGS data (more detail in Appendix A). The Pearson correlation coefficient for annual inflow between Farah and Hirmand Rivers during 1955-1980 is 0.82, meaning Hirmand River is a reasonable indicator of total inflow to Hamun Lakes (Figure S 1).

Available rain gauge data in the study area in Afghanistan and Iran do not have good spatial and temporal coverage. We used widely-used satellite-based rainfall products, namely GPCC (Schneider et al., 2011), PERSIANN-CDR (Ashouri et al., 2015) and TRMM (Huffman et al., 2007). All of these products show high amount of precipitation in the region in recent years (more detail in Appendix B). We used the GPCC rainfall data to estimate precipitation in Hirmand River sub-basin from 1960-2016, which has high correlation with PERSIANN (0.84) and TRMM (0.94). We calculated annual precipitation and flow data based on the Iranian water year from October to September. Digital elevation model (DEM) data are from ALOS World 3D - 30m (AW3D30) (Tadono et al., 2016).

2.3. Models

2.3.1. Water body detection

The Normalized Difference Spectral Indices (NDSIs) are commonly used for surface water detection (Akbari et al., 2020; Boschetti et al., 2014). Among different NDSIs, those using visible bands (such as red, green, etc.), near-infrared band and short wave near infrared band have been shown to outperform others (Boschetti et al., 2014). The Normalized Difference Vegetation Index (NDVI) and the Normalized Difference Water Index (NDWI) are two examples of this class of NDSIs, which facilitate water detection (Akbari et al., 2020; Chipman and Lillesand, 2007; Ouma and Tateishi, 2006;

Pekel et al., 2016; Rokni et al., 2014; Rouse Jr, 1973; Zaki et al., 2018). Both indices are based on normalized difference of bands in the electromagnetic spectrum and vary between -1.0 to 1.0:

$$NDWI = (NIR - SWIR)/(NIR + SWIR) \quad 1$$

$$NDVI = (NIR - Red)/(NIR + Red) \quad 2$$

where NIR, RED and SWIR are reflections in the near-infrared, red visible and short wave near infrared.

High NDWI and low NDVI values represent water and we need to define a specific threshold to determine water from non-water. We have access to multispectral remotely sensed products from different satellites, such as Sentinel, Landsat, and MODIS. We utilized MODIS images available after year 2001 because daily temporal resolution of this product helps resolve the common cloud cover issue by providing more images in each month. Furthermore, we used Landsat images available for the study area from 1987-2001 to expand our temporal coverage. We used MODSI NDWI and Landsat NDVI products due to their good quality in the study region to determine the monthly variation of water bodies' area. Also, $NDVI < 0$ and $NDWI > 0.1$ were considered as water using Google Earth Engine Java Script API (Gorelick et al., 2017) (the source code is provided in supplementary materials).

2.3.2. Hamun Lakes rate of desiccation

We quantified the monthly rate of desiccation (i.e. $d(area)\ /d(time)$) for Hamun Lakes when they receive no inflow. Monthly flow to Iran from Hirmand River was zero during March 1999 to August 2002, providing a suitable timeframe for the analysis. We used monthly area of all Hamun Lakes from Landsat and MODIS satellites during this period to estimate how fast Hamun Lakes desiccate after inflow cut.

2.3.3. Sensitivity of the Hamun Lakes area to monthly inflow from Hirmand River

The relationship between inflow to Hamun Lakes and the lakes' area was investigated based on NDWI monthly images and monthly inflow of Hirmand River to Iran from Jan. 1987 to Aug. 2013 when monthly inflow data is available. We defined three classes of monthly inflow: 1) inflow less than 0.5 km^3 (275 cases), 2) inflow between 0.5 and 1 km^3 (30 cases) and 3) inflow more than 1 km^3 (15 cases). We chose 0.5 km^3 as a threshold of runoff classes because this is approximately equal to the active capacity of CNR4 and water demand in the Sistan region. This approach allowed an investigation of how water demand and new water regulation capacity after CNR4 went into operation affected the area of the lakes.

2.3.4. Drought Indices (SPI and SDI)

Using annual (Oct. to Sep.) precipitation and runoff, we calculated Standardized Precipitation Index (SPI) and Standardized Discharge Index (SDI). To analyse the temporal hydro-climatological status of the Hirmand River sub-basin, the trend, the variation, and the average value of rainfall and discharge were calculated. Temporal climate variability was characterized using SPI, which is designed to evaluate metrological drought (McKee, 1995) and has been widely used for evaluating climate variability (Hao et al., 2014; Irannezhad et al., 2015). SPI requires fitting a probability density function (McKee, 1995; Thom, 1966) to the frequency distribution of precipitation at a given station for a particular timescale (e.g. 3 months and 6 months). In this study, annual SPI was estimated as (Farahmand and AghaKouchak, 2015):

$$SPI = \emptyset^{-1}(p) \qquad (3)$$

where $\emptyset$ is the standardized normal distribution function and p is the corresponding empirical probability when the precipitation in Hirmand River sub-basin are sorted in ascending order. Based on SPI, climate conditions can be divided into eight categories as classified in Table 1.

SDI calculation is like SPI, but we used Hirmand River flow to Iran instead of precipitation. SPI and SDI are used to describe various drought categories. Over time, increased water consumption typically occurs in the upstream part of many basins. Increasing upstream water withdrawal or land-use change which can significantly alter river flow, and subsequently downstream water delivery. We compared SPI and SDI to evaluate the possible link between rainfall and discharge variation (Shukla and Wood, 2008; Torabi Haghighi et al., 2020).

3. Results

3.1. Areal change of the lakes in the Sistan region

The monthly area of CNRs (Figure 2-e to h) shows that these reservoirs did not experience complete desiccation in all operating years except at the beginning of the 2000s due to extremely dry conditions (Table 1). Based on the monthly area boxplot in Figure 2-a to d, although monthly area variation in Hamun Lakes is high, sometimes nearing zero (i.e., complete desiccation), the CNRs exhibited low variation in monthly average area in all years of operation (box plots in Figure 2-e to h) with standard variation coefficients of 8.4%, 8.8%, 3.8% and 26.4% for CNR1 to CNR4, respectively.

Monthly area of the Hamun Lakes (Figure 2-a to d) shows that all of them lost most of their area after April-May and after April-May inflow reductions in the region (Figure 5-d). Gaud-i Zirreh desiccated completely (Figure 2-d) because inflow to Shile Canal was zero after 2000, causing the monthly areal change of this water body to be different from the other lakes (boxplot of Figure 2-d). CNR1, CNR2 and CNR3 also reached maximum area in April-May (boxplots in Figure 2-e to g) when Hirmand River deliveries to Iran increased (Figure 5-d). CNR4 is Iran’s last man-made reservoir in the series, receiving overflow from CNR1, 2 and 3 when these reservoirs are filled in April-May by spring flow. Thus, the area of CNR4 starts to increase after April-May. Based on the falling limb of the boxplots in Figure 2-e to g, the area of CNR1, 2 and 3 decreased in October, November and December because of conveying water to CNR4 (i.e., the rising limb of the boxplot shown in Figure 2-h). This operation strategy prepares CNR1, CNR2 and CNR3 to capture inflow in April-May by lowering the water level in CNR1 to maximize the discharge of the Feeder Canal (Figure 1-d), which is why the area of CNR4 is the highest during this period.

After April-May, the lakes' area gradually decreased to less than 5% of maximum value due to low inflow (falling limb of monthly inflow hydrograph in Figure 5-d) and high evaporation rate in the desert climate. Based on available images from Landsat and MODIS satellites from 1987-2020 (Figure 2), after 1990, all the Hamun Lakes had a large area because the highest inflow of Hirmand River to Iran since 1960 occurred in 1990 (Figure 1-e). After the onset of a severe drought period in 1999 ($SDI = -1.5$) and 2000 ($SDI < -2$), shown in Figure 5-a, the annual maximum area of Hamun-i Puzak, Hamun-i Sabari did not change considerably, but the duration of complete desiccation was longer (Figure 2-a and b). On the other hand, Hamun-i Hirmand almost dried up (lower maximum annual area and longer complete desiccation in Figure 2-c). Gaud-i Zirreh (depth: $\approx$10 m), which is more than 5 times deeper than the other lakes, is the only water body in this system that did not completely desiccate immediately after the severe drought of 1999-2000 and 2001-2002 (SDI close to -2).

3.2. Rate of desiccation of Hamun Lakes

At the beginning of March 1999, Hamun-i Hirmand was 950 km^2, i.e. half the maximum area based on available satellite images since 1987. Hamun-i Hirmand dried out over the next 8 months when inflow to Hamun Lakes was zero (Figure 3). The slope of the desiccation line was lower when the lake's area was between 950-700 km^2 compared with when the area ranged from 700-0 km^2, which means the shrinkage process accelerates as the water body becomes smaller (Figure 3). Hamun-i Puzak and Hamun-i Sabari took 17 months to dry up. The rates of desiccation (slope of lines shown in Figure 3) in Hamun-i Puzak, Hamun-i Sabari, and Gaud-i Zirreh are higher, but they become smaller. Gaud-i Zirreh is more resistant to inflow cut-- Shile Canal inflow was zero after 2000--and its complete desiccation takes about 6 years to happen (70 months) due to higher depth of this lake compared to other Hamun Lakes.

3.3. Water flow through Hamun Lakes

We chose the 1988-1991 period to demonstrate how Hamun Lakes fill up and connect to each other (Figure 4); since in this period the lakes change from almost completely dry to full as captured by satellite images. The year 1988 ($SDI = 0.7$) was a transition year from the 1983-1987 dry period ($SDI < 0$ except 1985 when $SDI = 0.2$) to a very wet year in 1989 ($SDI = 1.1$) and an extremely wet year in 1990 ($SDI > 2$).

In the first months of 1988 (mildly wet), the Hamun Lakes were nearly empty due to the preceding drought period. The water area in the Northern Hamun Lakes started to increase in January to May by inflow in the same month but Gaud-i Zirreh kept shrinking because the level of water in northern Hamuns were not enough to feed the Shile Canal (compare Figure 4, 1988-03 and 1988-05; also overflow between northern Hamuns is observable). All the Hamun Lakes shrank (Figure 4, compare 1998-05 and 1988-07) during May-November 1988 due to reduced inflow in May (to almost zero) and water loss to evaporation. Inflow in December 1988 and January 1989 raised the water area in the northern lakes (Figure 4, compare 1988-12 and 1989-02) immediately. A similar pattern is observed in 1989 (very wet year) when inflow was enough to reach Hamun-i Hirmand, although the Shile Canal and consequently Gaud-i Zirreh were not fed (Figure 4, 1989-04). In 1990 (extremely wet year), inflow was the highest since 1960 and Shile Canal delivery increased the water area in Gaud-i Zirreh (Figure 4, 1990-01). When inflow decreased in May 1990, the shallow lakes upstream of the Shile Canal, lost considerable area immediately. Expectedly, it took longer for deeper portions of the cascading lakes to desiccate in response to decreased inflow.

In March 1991 maximum recorded inflow (4.5 km^3) of the Hirmand River entered Iran. Max area for Hamun-i Puzak (1300 km^2) and Hamun-i Sabari (1500 km^2) was observed in this month but the maximum area of Hamun-i Hirmand (1800 km^2) occurred one month later (April 1991). The area of Hamun-i Hirmand in March 1991 was 1700 km^2. The largest area for Gaud-i Zirreh in 1991 was 2600 km^2 observed four months later in July. Therefore, the time lag for water conveyance from Hamun-i Puzak and Hamun-i Sabari to Hamun-i Hirmand and finally to Gaud-i Zirreh was almost one and four months, respectively. Additionally, the maximum area of Gaud-i Zirreh was 3000 km^2, which occurred more than 25 months later (in June 1993) because of accumulating inflow volume in preceding years.

3.4. Drought in the Hirmand River sub-basin

The analysis of the correlation between SPI and SDI in the years before and after 2004, which are 0.66 and -0.52 respectively, reveals a drastic change in the inflow of the Hamun Lakes. Before 1990, SDI values were almost always (all the years in the record except 1962 and 1984) larger than SPI values (on average 0.65 larger) (Figure 5-a). However, after 1990, the SDI was lower than SPI (blue point in Figure 5-a) excluding 1994, 1998, 1999 and 2005. The average difference between SDI and SPI was -0.9 after 1990, which increased to almost -2 after 2004 (Figure 5-a). Based on Table 1, a difference equals to -2 between these two indices will considerably affect the classification of the year to dry or wet state. In other words, when SPI is about 2, indicating an extremely wet year, the SDI can be less than 0, which is characteristic of a dry year.

The mean annual precipitation in the whole Hirmand sub-basin (Figure 1-a) has the highest correlation with the precipitation upstream of Kajaki Dam (≈ 0.97, Figure S 4). The mean precipitation in the Hindu Kush mountainous region is higher than other parts of the basin (Figure S

3-b); however, the correlation between precipitation in mountainous parts of the basin and lower regions downstream of Kajaki Dam is low ($\approx 40\%$). In other words, according to SPI, the wet and dry cycles in the Hirmand sub-basin are governed by precipitation amounts in the upper parts of the sub-basin rather than downstream of Kajaki Dam (Appendix B). This means that we may observe wet conditions in upstream of Kajaki Dam but dry conditions in terms of precipitation in downstream of Hirmand River. High climatic variation of the Helmand Basin is important because most of the runoff formed in the upstream wet snow climate (Ds) and warm temperate climate (Cs) will determine the area of Hamun Lakes in the lower desert climate (BW). Also, the monthly distribution of precipitation in the Helmand Basin shows that March is often the wettest month of the year (Figure 5-d) even though the highest inflow to Iran is more frequent to occur with some time lag in April or May (more detail in Appendix C).

3.5. Impact of reservoir construction in Iran

The capacity of CNR4 is more than 0.8 km^3, i.e. 40% of annual Hirmand River flow into Iran in the last 10 years. This reservoir has more than doubled the water regulation capacity in the region from 0.65 to 1.45 km^3, which can affect the area of the Hamun Lakes. In this regard, we determined the effect of CN4 on the state of the lakes' area by comparing similar hydrological conditions in different years when Hirmand River deliveries to Iran were almost the same before and after operation of CNR4, i.e. 1992/2016, 1996/2009 and 1993/2011 (Figure 6- to c).

In 1992 ($inflow \approx 4$ km^3), the area of Hamun-i Hirmand, Hamun-i Sabari and Hamun-i Puzak were 1600, 1500 and 1000 km^2, respectively, which decreased by 55, 43 and 87% in a similar condition in 2016 after the construction of CNR4 (Figure 6-a). This demonstrates that the construction of CNR4 in Iran has worsened the situation of the Hamun Lakes in addition to the upstream water regulation in Afghanistan. In 2009 ($inflow \approx 2.5$ km^3) Hamun-i Hirmand lost 86% of its area compared to 1996

(Figure 6-b). The areal loss of this lake in 2011 ($inflow \approx 2$ km^3) was 95% compared to 1993 (Figure 6-c). Likewise, the area of Hamun-i Puzak and Hamun-i Sabari decreased 57 and 45% in 2011 compared to similar conditions in 1993 (Figure 6-c). In 2009, the area of Hamun-i Sabari and Hamun-i Puzak were less affected by CNR4. In this year, only 19 and 11% of these lake's areas, respectively, were lost compared to 1996 (Figure 6-b). There are no streamflow data available for other rivers that feed to Hamun Lakes but water presence in a wetland in the northeast of Hamun-i Puzak (Figure 6-b) shows considerable inflow from Khash River and likely other rivers in the north (Figure 1-b). Since 2009, more than 70% of this wetland was full (even more than its area in 1996). However, the wetland was dry in all other years after CNR4 operation and 2009 is an exception. Based on our investigation, Hamun-i Hirmand is more sensitive to the impact of CNR4 than Hamun-i Sabari and Hamun-i Puzak.

3.6. Monthly response of Hamun Lakes area to Hirmand River flow

Monthly inflow can largely affect the area of Hamun-i Puzak and Hamun-i Sabari in the same month (Figure 7-a and b) since water retention time in connected Hamun Lakes above Shile Canal is small due to their low depth (shown in Figure 3 and Figure 4). When monthly Hirmand flow to Iran is less than 0.5 km^3, the area of Hamun-i Puzak is most likely to be less than 500 km^2 (Figure 7-a). Also, when inflow increases from 0.5 to between 0.5-1 km^3, the area is more probable to exceed 500 km^2. Also, the area of this lake increases to more than 1250 km^2 when the Hirmand River delivery to Iran exceeds 1 km^3 (Figure 7-a). Hamun-i Sabari is expected to be larger than 500 km^2 when inflow to Iran rise from below 0.5 to above 0.5 km^3. Likewise, greater areas than 500 km^2 are expected for Hamun-i Hirmand when inflow increases (Figure 7-c). Boxplots of Hamun-i Hirmand and Gaud-i Zirreh have a considerable overlap (Figure 7-c and d) so there is no specific relation between Hirmand River inflow to Iran and their area in the same month. The areas of Hamun-i Hirmand and, especially Gaud-i Zirreh were very low after 2000 (Figure 2-c and d), indicating that Hirmand River inflow does not reach these lakes and such comparison is not possible. Also, Gaud-i Zirreh has higher water retention time which resulted in higher dependence of this lake's area to previous months, i.e. water accumulation from preceding months.

4. Discussion

Hamun Lakes are responding to a shift in water management paradigm in a transboundary basin where competition over limited water resources is on the rise. The new paradigm is intensified after 2004 which has marginalized environmental flows to the lake as detected by high gap between SDI and SPI. The lakes are experiencing exacerbated environmental flow stress mainly due to human modifications and flow regulation. The continuation of this trajectory is expected to amplify adverse environmental, socio-economic, and public health impacts associated with more frequent and prolonged desiccation of the lakes. The unfolding environmental consequences of water bodies loss have heightened public and political sensitivity. It is urgent to recognize environmental water security as an important element of region's sustainability and plan practical steps to increase binational cooperation to prevent extensive socio-ecological impacts.

Increased regulation of Hirmand River flow in this transboundary basin has weakened the hydrologic conditions to sustain the lakes. Based on the inflow of Hirmand to Iran, three major hydrological droughts occurred in the 1970s, 1980s and 2000s (Figure 1-e). These droughts prompted the Iranian government to sign the WP with Afghanistan in 1972, and construct CNR1, CNR2 and CNR3 in 1983, and CNR4 in 2008 (Figure 1-d) to store more water to meet regional demand. The cumulative capacity of CNRs ($\approx$ 1.5 km^3) plus 0.3 km^3 of annual evaporation from their surfaces made up almost 95% of the total annual inflow of Hirmand River to Iran from 1995-2016, $\approx$ 1.9 km^3 shown in Figure 1-e. While CNRs have been effective in helping meet the water demand in the Sistan region, they have caused a decline in the area of the Hamun Lakes. Furthermore, four dams in Afghanistan

(Figure 1-a) with a collective water storage capacity of more than 3 km^3 heavily regulate the flow. The lakes' area is declining although Hirmand River inflow to Iran has averaged 1.9 km^3 in recent years, more than double the designated WP delivery. This indicates that temporal patterns of deliveries from Afghanistan and human water demand on the Iranian side make water deliveries to the lakes challenging.

The high correlation between SPI and SDI from 1960-2003 shows that high precipitation naturally will lead to high runoff in the Hirmand River sub-basin. The large discrepancy between SPI and SDI after 2004 is a strong evidence about the effects of recent anthropogenic modifications on the Hamun Lakes. Water regulation upstream of the Hirmand River in Afghanistan has become more intensive, decreasing the deliveries to Iran as a new phenomenon in the basin. Before 2010, the maximum recorded annual precipitation of the Hirmand River sub-basin was 330 mm in 1990, which led to the maximum flow into Iran since 1960 (i.e., 12 km^3). While the annual precipitation in 2015 (473 mm) was 40% larger than the 1990 rainfall, the Hirmand River inflow to Iran in this year was 30% of the flow delivered in 1990 (i.e., less than 4 km^3), indicating greater upstream regulation in Afghanistan.

The large area of CNRs (Figure 2-e to h) in all years (except dry years in 2000 and 2001) regardless of the SDI value is an artifact of the priority given to filling the CNRs as much as possible to meet water demands in the Sistan Region, Iran. Once CNRs are full, the overflow is conveyed to Hamun Lakes. Low monthly areal variation of CNR4 compared to Hamun Lakes denotes the importance of CNRs for water supply in Iran, which is an impetus for more than doubling the capacity of the CNRs in 2008 by adding CNR4. Increasing the monthly inflow by 0.50 km^3 to Hamun Lakes can affect their monthly area, especially in Hamun-i Puzak and Hamun-i Sabari (Figure 7). This illustrates the environmental water stress caused by diverting 0.820 km^3 to store in CNR4, which can severely impact the area of the lakes above Shile Canal (Figure 6) because it further reduces the already dwarfed Hirmand flow due to more intensive upstream regulation in Afghanistan.

The effects of increased water regulation propagate back into Afghanistan in lower elevation downstream most sections of the basin. Gaud-i Zirreh, which is more resistant to desiccation than other lakes, nearly dried out after 2005 prior to the operation of CNR4. For example, although, inflow in 1993 is less than 1992, Gaud-i Zirreh area is highest in 1993 ($\approx$3000 km^2) because accumulated water from extremely wet (1990: $inflow \approx 12$ km^3) and mildly wet (1991: $inflow \approx 5$ km^3 and 1992: $inflow \approx 4$ km^3) years. Therefore, the desiccation of Gaud-i Zirreh should be also attributed to Hirmand River regulation in Afghanistan (annual inflow decreased from 4 to 1.9 km^3 shown in Figure 1-e) which is worsen by Iran reservoir construction.

The 1999-2002 drought was the most severe on record going back to 1830 (Williams-Sether, 2008). After this dry period, the frequency and severity of dust storms has significantly increased (Rashki et al., 2012). This affects the livelihood of more than 1.1 million people who rely on Hirmand River inflow and Hamun Lakes in the Sistan region (Rashki et al., 2013). More than 25% of the population migrated from Sistan region due to environmental and economic situation after Hamun Lakes desiccation (ICANA, 2015). In 1977 more than 55% of Sistan inhabitants in Iran worked in the agricultural sector but this ratio has reduced to less than 22% in 2015 due to water scarcity and droughts (Ministry of Cooperatives Labour and Social Welfare Iran, 2017). Drought has negatively impacted fisheries which have been brought to a halt (Rashki et al., 2012) and caused high unemployment (ICANA, 2012). The unemployment and declining quality of life can undermine border security due to potential links to unlawful economic activities, and in some cases terrorism (Bagchi and Paul, 2018).

Lack of in-situ data such as inflow of Khash, Farah and Adraskhan Rivers, precipitation, water diversions to farms are sources of uncertainty in this study due to the use of proxy variables. For example, the area of a wetland in the east of Hamun-i Puzak was used to assess the Khash River inflow status. Additionally, while satellite data products help address data limitations to a great extent, they also introduce uncertainties because of their coarse spatial and temporal scales. The thresholds for detecting water by NDVI (< 0) and NDWI (> 0.1) were selected based on ground observations of Gaud-i Zirreh area, which has declined to almost zero in recent years, having received minimal inflow after 2000 based on Pol-Shile station flow record. The use of two different satellite data streams (i.e., MODIS and Landsat) for water detection helps reduce uncertainties by minimizing the effect of cloud cover on available images.

5. Conclusions

Hamun Lakes are connected water bodies consisting of three connected Lakes (Hamun-i Puzak, Hamun-i Sabari and Hamun-i Hirmand) above Shile Canal and a deeper terminal lake (Gaud-i Zirreh). The first three cascading lakes are very shallow, and they respond rapidly to monthly Hirmand River inflow variation. The area of these lakes is considerably affected by increased water storage in Iran (i.e., Chah Nimeh Reservoir 4 with a capacity of 0.820 km^3). The negative effect of surface water storage is intensified by high rate of evaporation in the Chah Nimeh Reservoirs (> 0.3 km^3), which supply water for human use in a socio-economically disadvantaged region of Iran. In addition, a shift in upstream regulations of the Hirmand River in Afghanistan has changed post-2004 water deliveries at the international border. From 1960 to 2003, Standardized Discharge Index (SDI) and Standardized Precipitation Index (SPI) were highly correlated (66%), meaning high river flow was expected to feed the lakes due to high precipitation over the basin. However, the correlation changed to -52% after 2004, indicating a drastic decline in the Hirmand River flow at the border despite large amounts of upstream precipitation, including the largest on record. The decline of the socio-ecological system due to unsustainable water management in this transboundary region is expected to have detrimental impacts on the socio-economic condition of the residents by increasing unemployment. The situation will also have important implications for public health due to more frequent dust storms. Although geopolitically challenging, revisiting the 1973 treaty between the two riparian states (known as Water Protocol) to provide environmental flows as a component of border environmental security, especially during dry periods, will create opportunities for improving the condition of the Hamun Lake system.

Acknowledgement

The authors are thankful to Dr. Kaveh Madani for his valuable comments. The second author acknowledges the Iranian and Persian Gulf Studies professorship from Oklahoma State University's School of Global Studies and Partnerships.

Funding

This work was supported by University of Oulu Graduate School (UniOGS). Furthermore, the authors have no conflicts of interest to disclose.

Data Availibility

All Google Earth Engine Java Script API source codes are available below:

- For extracting DEM and Urban:
  https://code.earthengine.google.com/fd8607d4c9d79f1ae6ae6d712877c877?noload=true
- For monthly and annually water body detection from 1987 to present:
  https://code.earthengine.google.com/76d2a59d4b05979fc583bd16573fc65e?noload=true
- For precipitation calculation:
  https://code.earthengine.google.com/5e14fcbbff9e0828b698340f58eb9628?noload=true

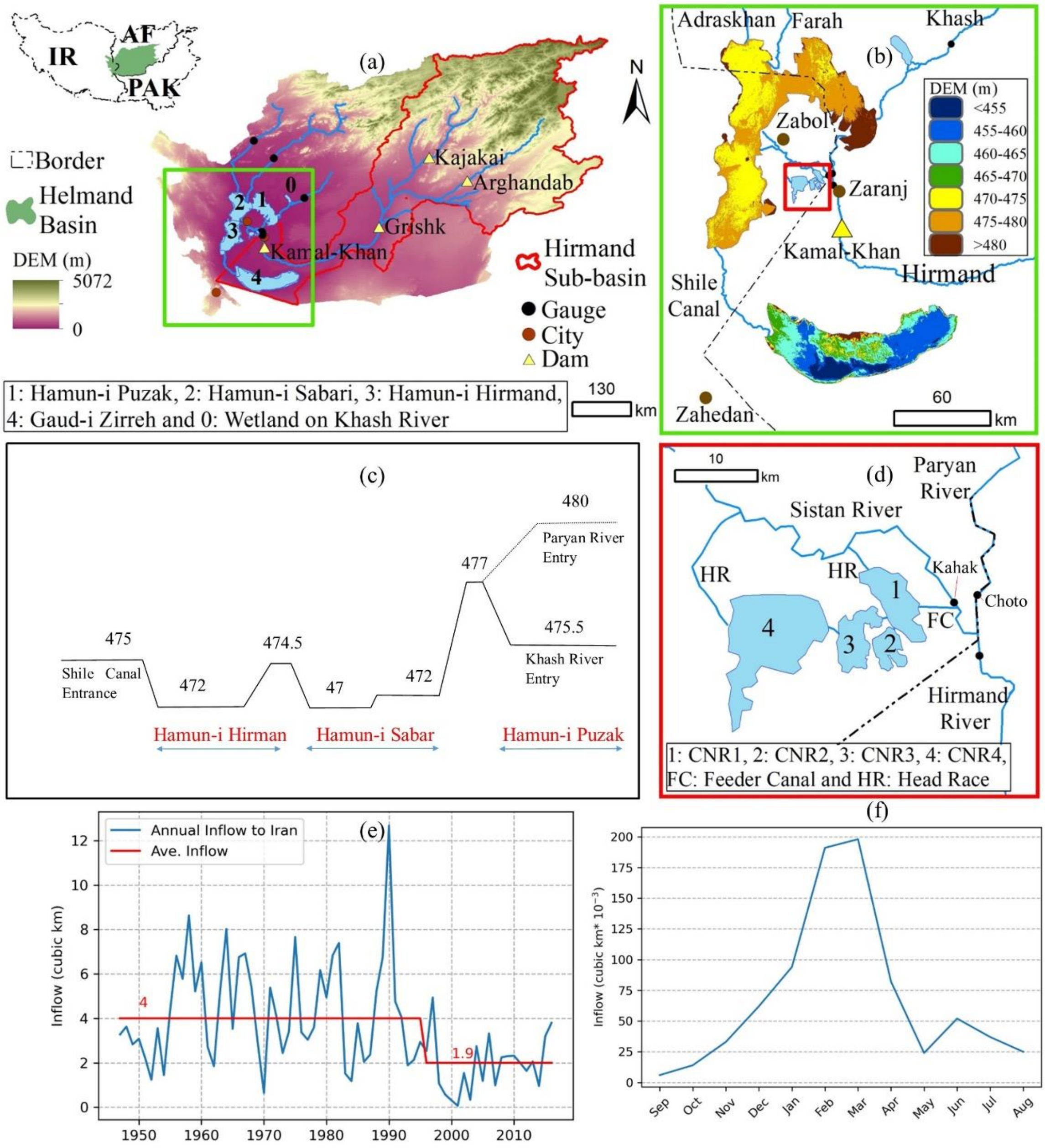

Figure 1. Studied area: a) Helmand Basin, Hirmand River sub-basin and Hamun Lakes with the location of dams, inflow gauges and cities, b) DEM of Hamun Lakes and close water bodies to Hamun Lakes, c) transverse profile of Hamun Lakes HIWRI, 2017), d) Hirmand, Sistan and Paryan Rivers next to border between Iran and Afghanistan, CNRs, Head Races and Feeder Canal and e) Annual inflow of Hirmand River to Iran from 1960 to 2016 and f) Water Protocol on Hirmand River inflow to Iran (ref: MoE, 2013)

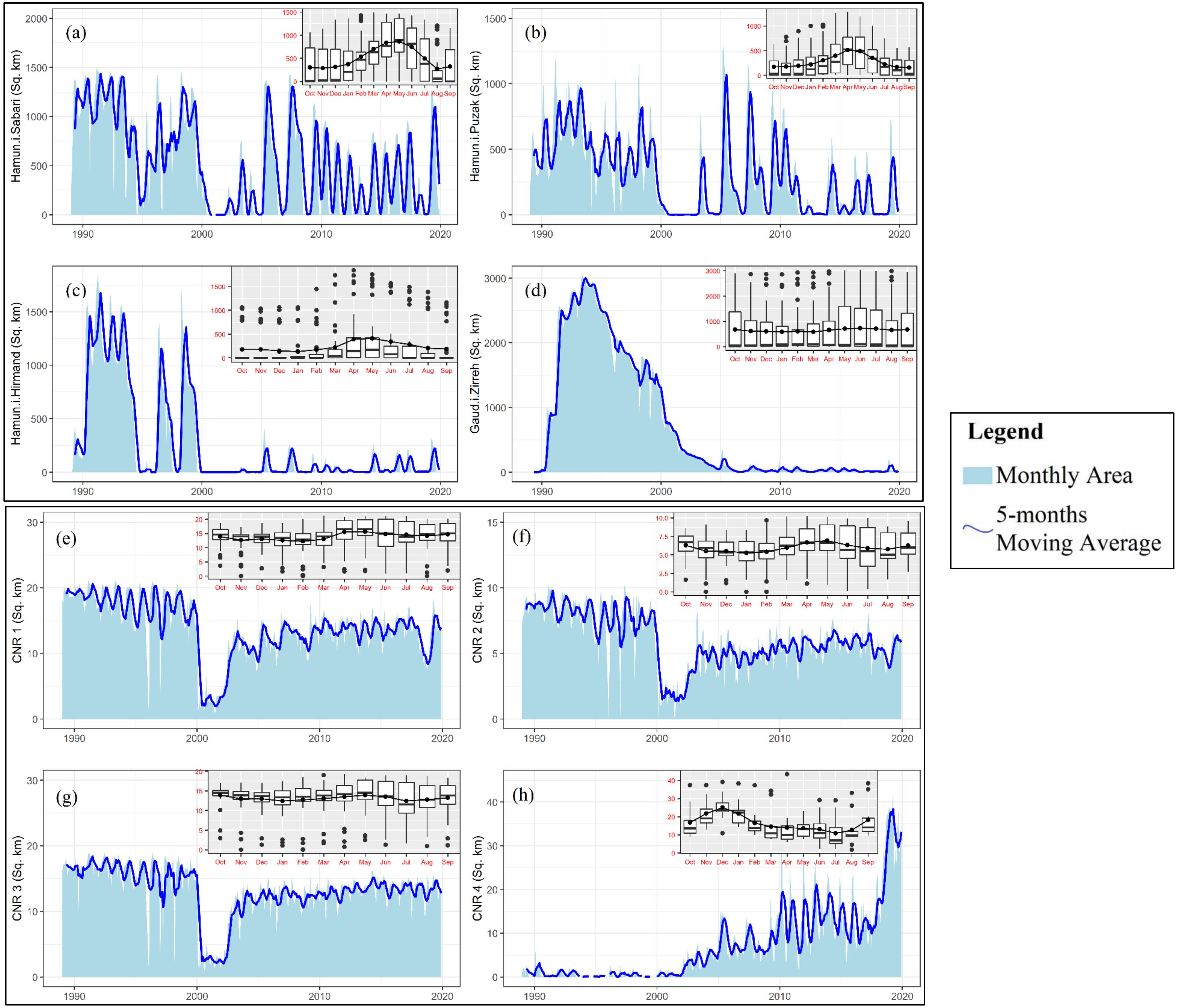

471 Figure 2. Monthly area with box plot of area in each month for: a) Hamun-i Sabari, b) Hamun-i Puzak, c) Hamun-i Hirmand, d) Gaud-i Zirreh, e) CNR1, f)
472 CNR2, g) CNR3 and h) CNR4

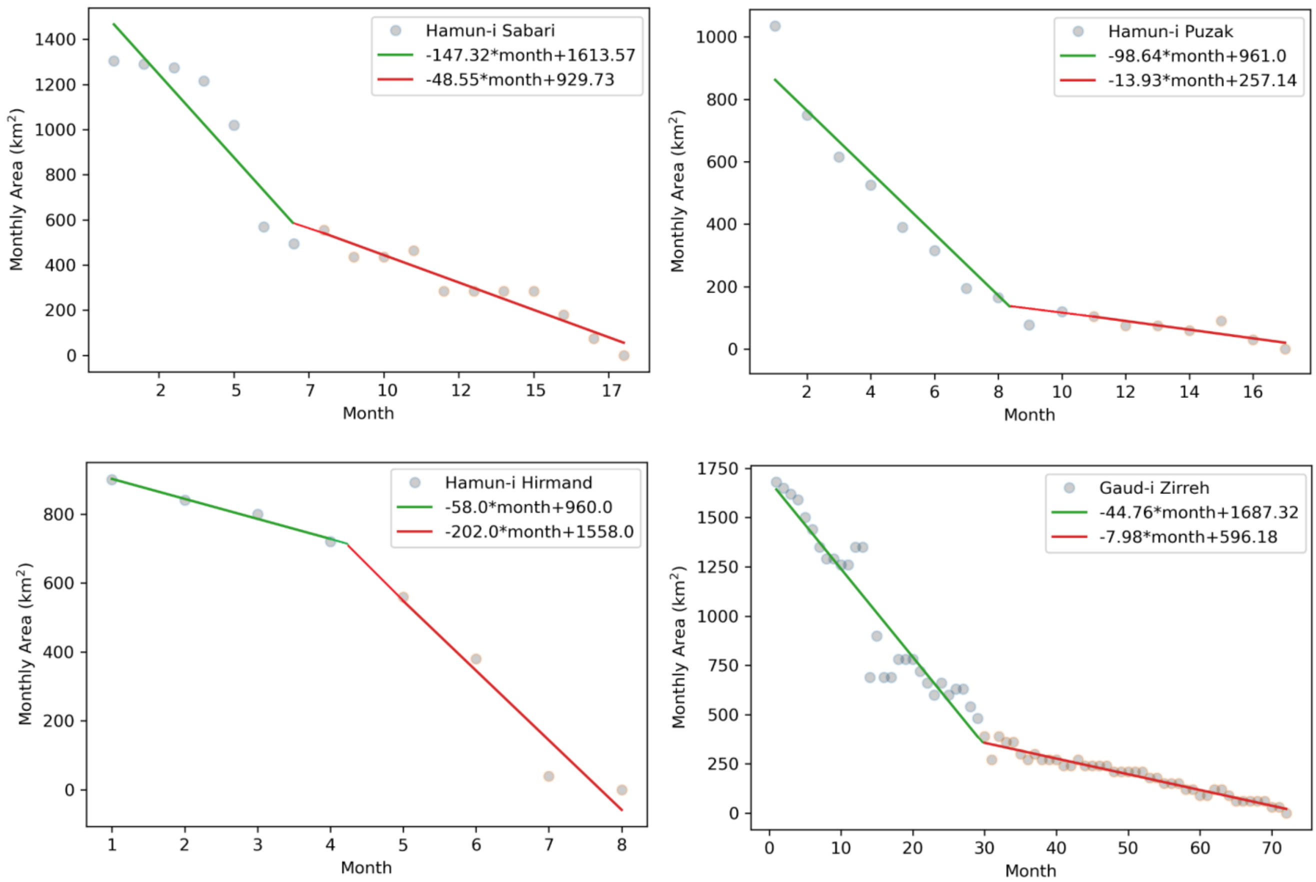

Figure 3. Desiccation of Hamun Lakes rate based on number of months passing from March 1999 when inflow became zero to each of lake

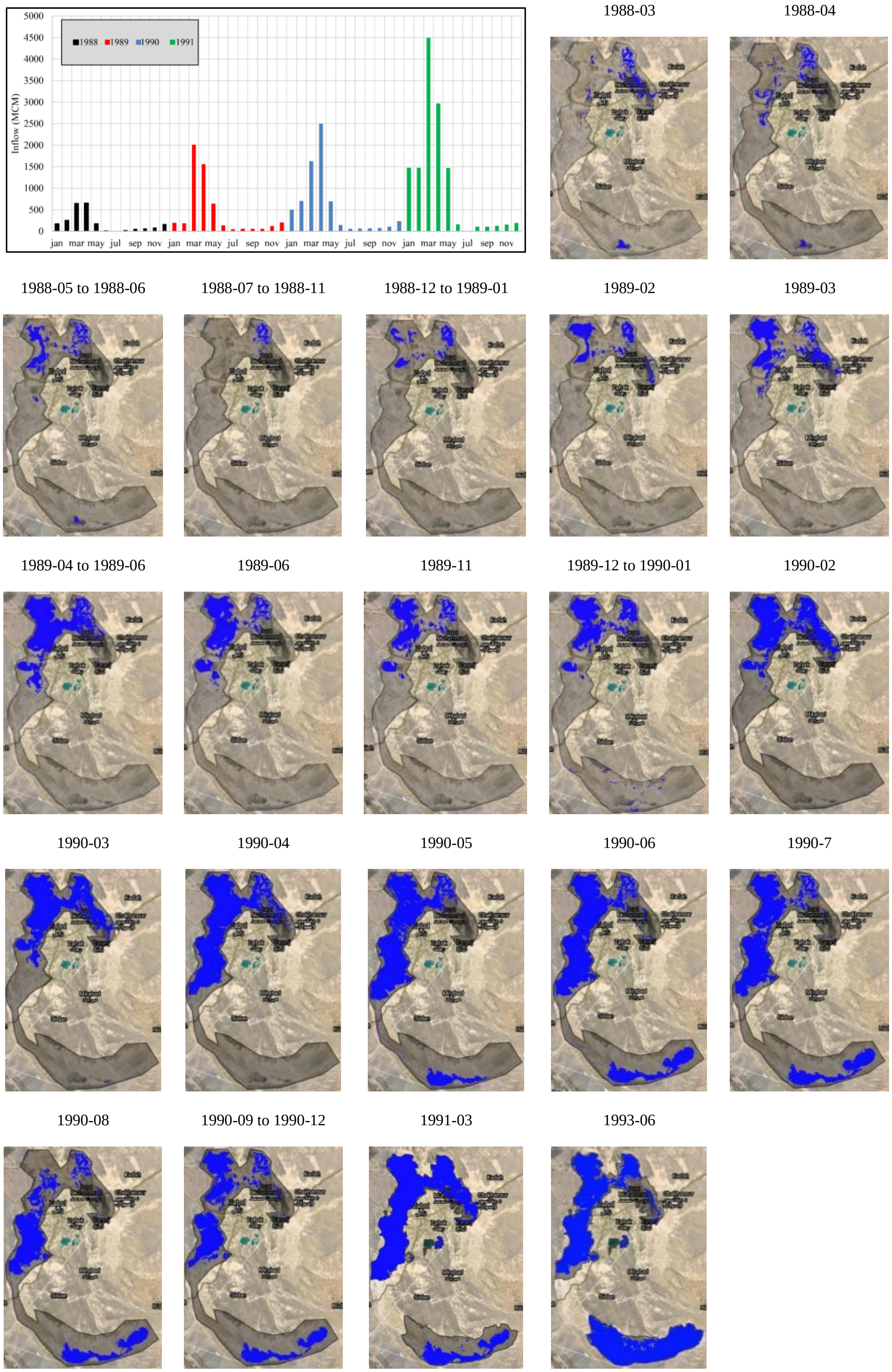

Figure 4. Water transfer between Hamun lakes (images are produced by Google Earth Engine Java Script API)

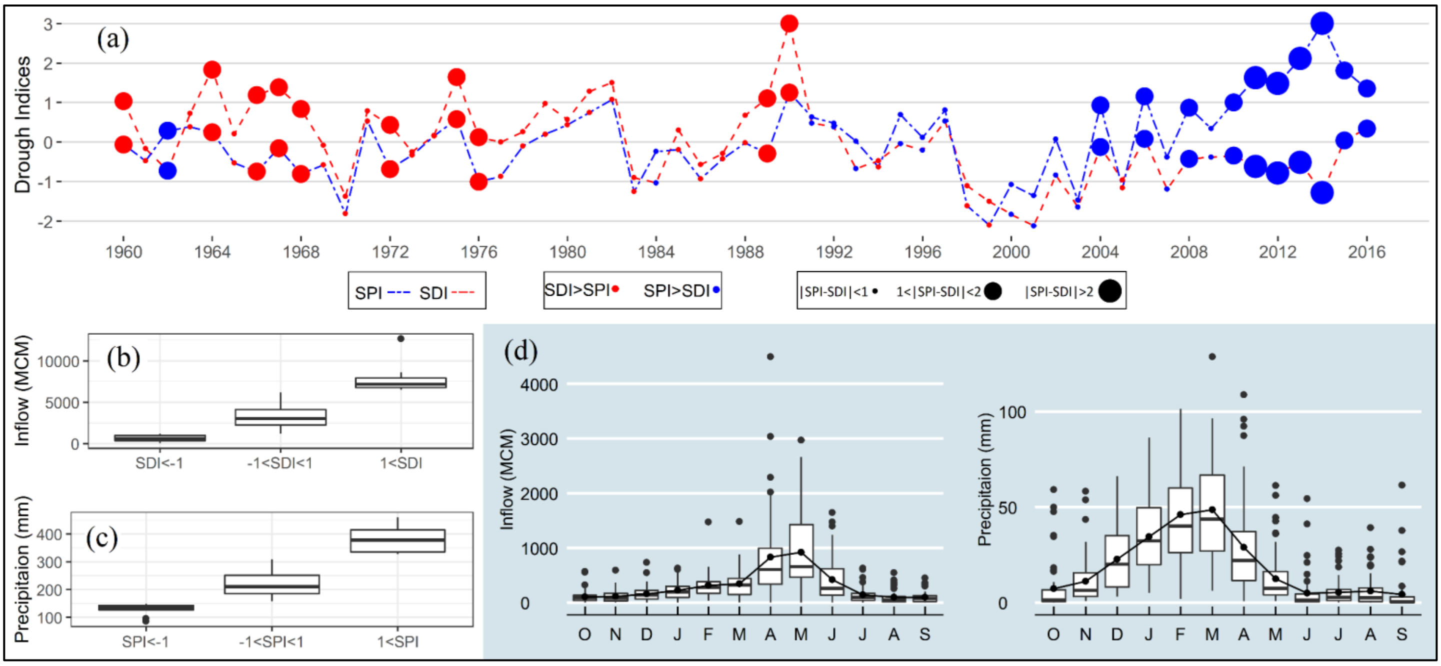

Figure 5. a) SPI and SDI of Hirmand River sub-basin from 1960 to 2016 with difference of SPI and SDI in each year showing a shift in water management paradigm after 2003 when high precipitation does not correspond to high Hirmand inflow to Iran, b) annual precipitation based on different intervals for SPI c) annual inflow based on different intervals for SDI and d) monthly distribution of Inflow and precipitation

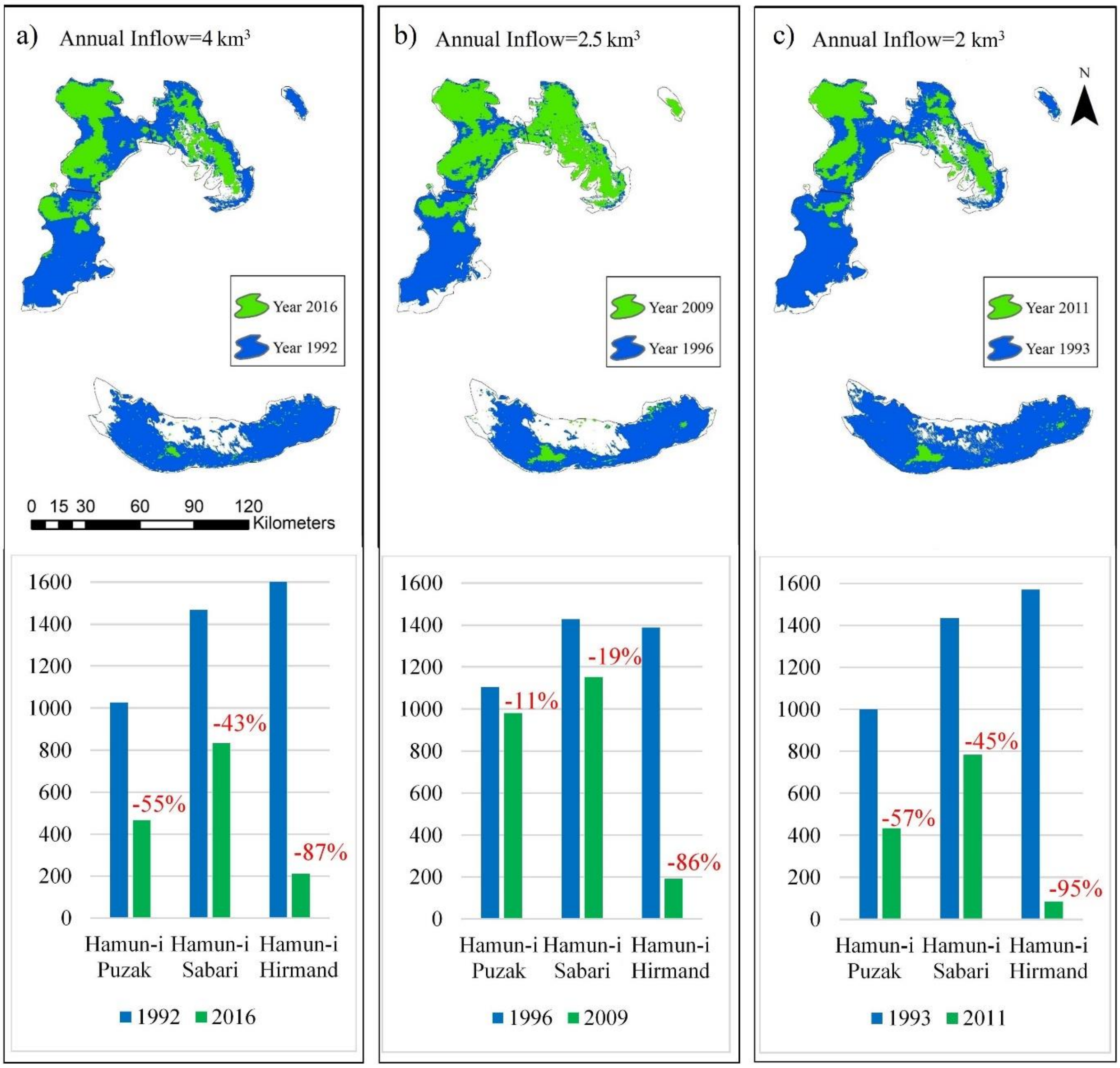

Figure 6. Effect of CNR 4 based on same annual inflow resulted in different areas for Hamun Lakes; percentage of negative effects on area decrease are shown in each bar plot

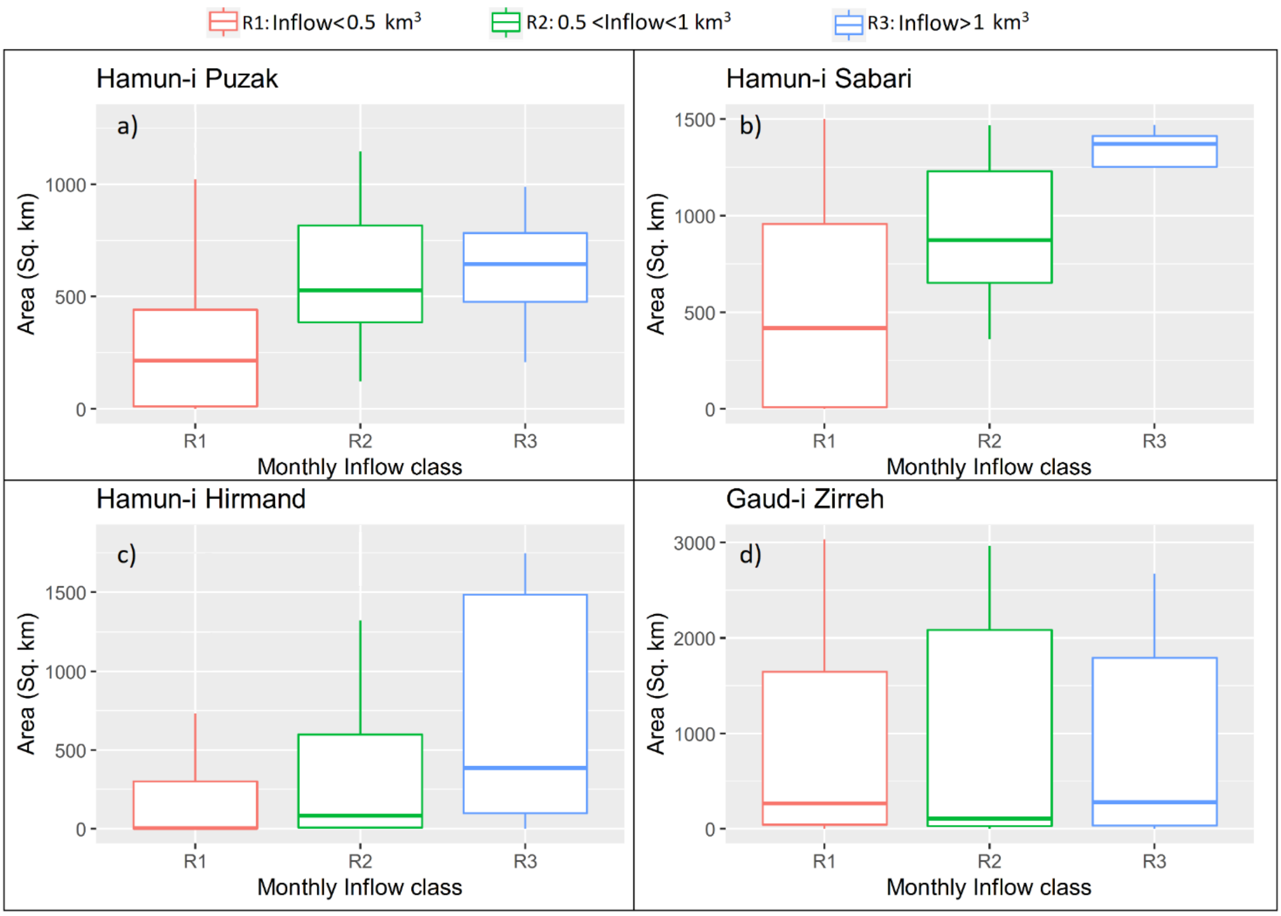

489

490 Figure 7. Consequence of incrementally increasing Hirmand River inflow by 0.5 km^3 on area of
491 Hamun Lakes

492

Table 1. Different categories of climatological conditions based on the drought indices (SPI/SDI) values

Category	*Range of drought indices (SPI/SDI)*
Extremely wet	More than 2.00*
Very wet	1.50–1.99*
Moderately wet	1.00–1.49*
Mildly wet	0.00–0.99*
Mild drought	–0.99 to 0.00*, **
Moderate drought	–1.49 to −1.00*, **
Severe drought	–2.00 to −1.50*. **
Extreme drought	<−2.00*, **

**Lloyd-Hughes and Saunders (2002). **McKee et al. (1993).*

Appendix A. Inflow of main rivers of Helmand Basin

Köppen-Geiger climate classification map in Helamad Basin and location of main rivers and their last gauges area shown in Figure S 1-a. Inflow of main rivers of Helmand Basin in Afghanistan observed in last gauges of each of them are also shown in Figure S 1-b based on USGS (Williams-Sether, 2008).

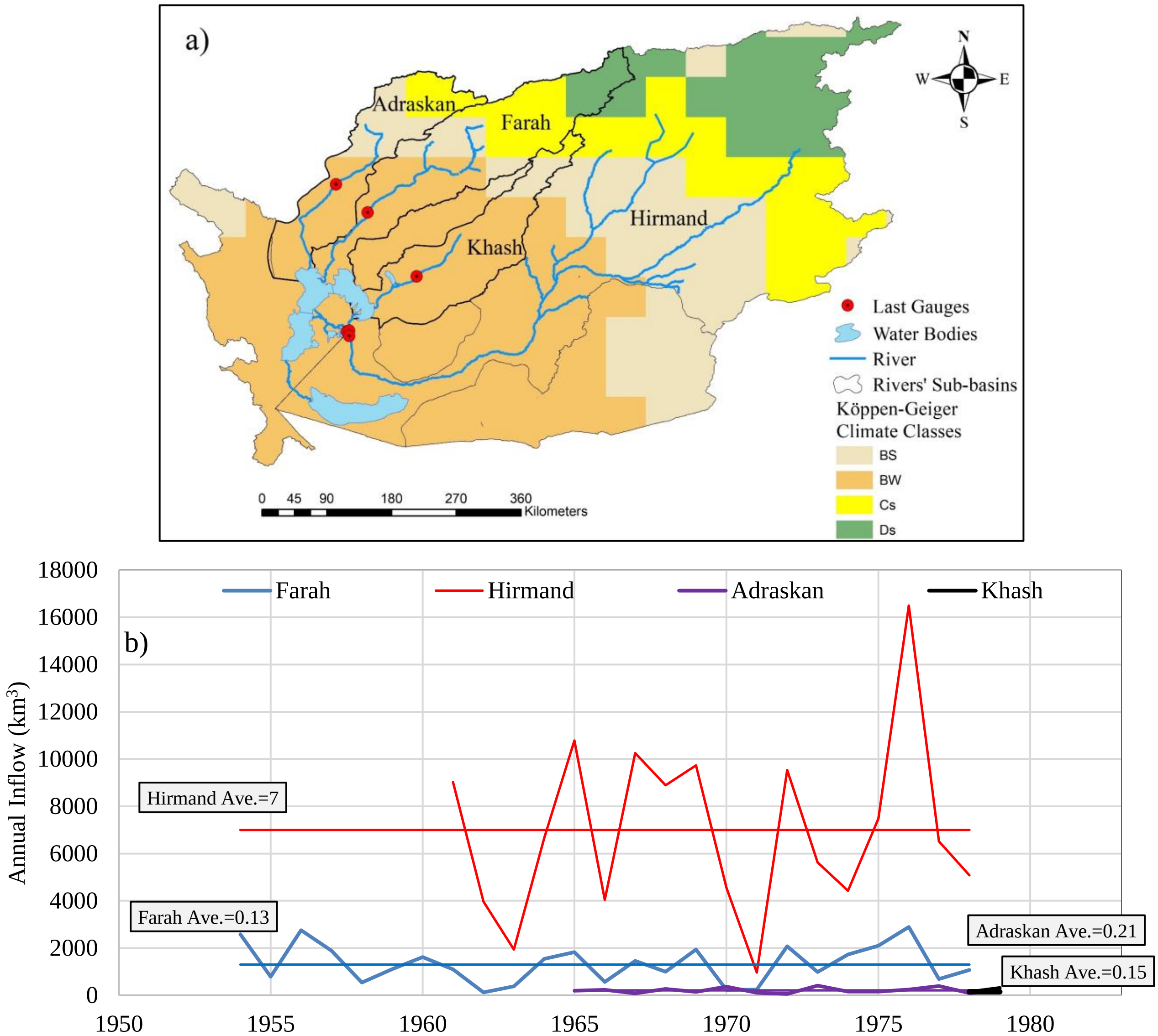

Figure S 1. a) Main rivers of Helamad Basin, their sub-basins with the location of last gauges on each of them and Köppen-Geiger classification map, b) Inflow of main rivers of Helmand Basin in Afghanistan observed in last gauges of each of them (retrieved from https://afghanistan.cr.usgs.gov/water)

Appendix B. Precipitation in Hirmand River sub-basin

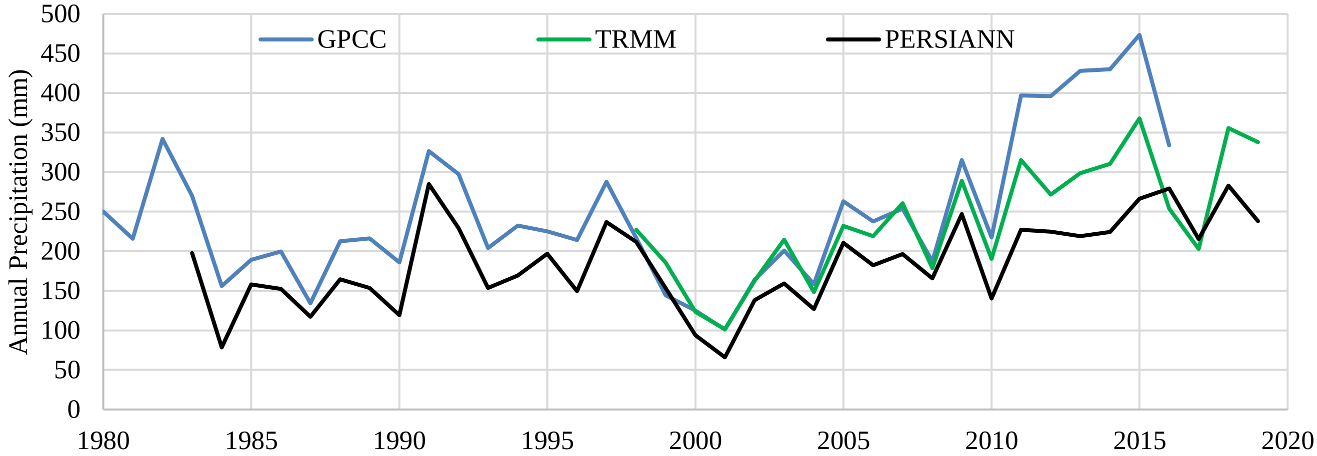

Figure S 2. Annual precipitation over Hirmand River sub-basin by different satellite products

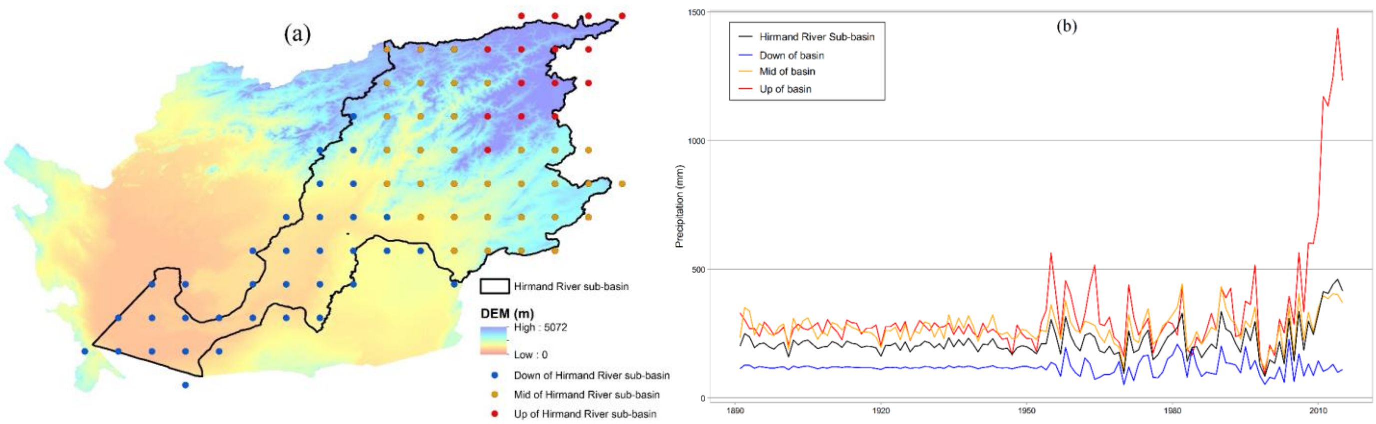

Figure S 3. a) Hirmand River sub-basin and DEM of Helmand Basin used to divide it to three regions: Up, Mid and Down based on elevation of regions, b) precipitation in all Hirmand River sub-basin, up, mid, and down regions calculated by GPCC

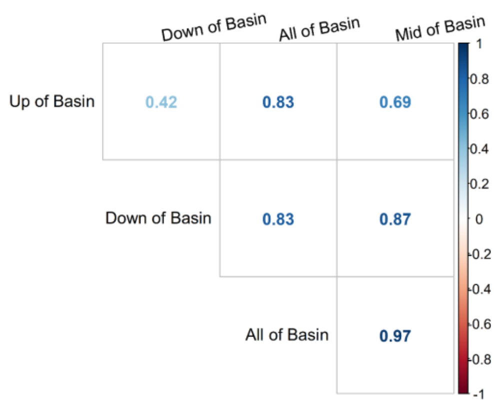

Figure S 4. Correlation of annual precipitation in different regions of Hirmand River sub-basin

Appendix C. Monthly inflow and precipitation

Precipitation is over Hirmand River sub-basin calculated by GPCC and inflow is measured in first gauge on Hirmand River in Iran next to border of Iran – Afghanistan. Based on below plots, 3rd quantile of precipitation in years with $SPI > 1$ is higher in Oct., to Jan.

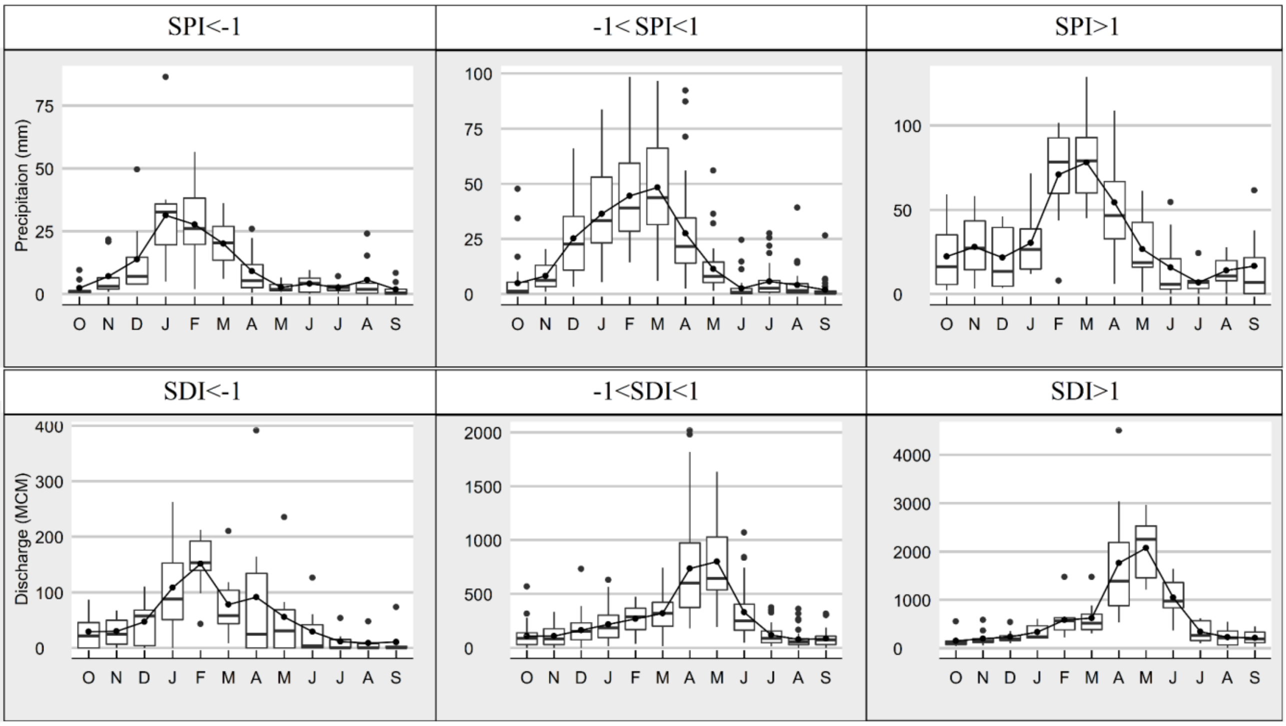

Figure S 5. Monthly distribution of precipitation and inflow in different years in terms of SDI/ SPI change

References

Absaran Consulting Company, 2015. Chah Nimeha water resources planning report, studies of the second phase of water supply in Sistan plain.

Afganistan Ministry of Urban Development Affairs, 2015. The State of Afghan Cities Report 2015.

AghaKouchak, A., Norouzi, H., Madani, K., Mirchi, A., Azarderakhsh, M., Nazemi, A., Nasrollahi, N., Farahmand, A., Mehran, A., Hasanzadeh, E., 2015. Aral Sea syndrome desiccates Lake Urmia: call for action. J. Great Lakes Res. 41, 307–311.

Ahlers, R., Brandimarte, L., Kleemans, I., Sadat, S.H., 2014. Ambitious development on fragile foundations: Criticalities of current large dam construction in Afghanistan. Geoforum 54, 49–58. https://doi.org/10.1016/j.geoforum.2014.03.004

Akbari, M., Baubekova, A., Roozbahani, A., Gafurov, A., Shiklomanov, A., Rasouli, K., Ivkina, N., Kløve, B., Haghighi, A.T., 2020. Vulnerability of the Caspian Sea shoreline to changes in hydrology and climate. Environ. Res. Lett.

Akbari, M., Torabi Haghighi, A., Aghayi, M.M., Javadian, M., Tajrishy, M., Kløve, B., 2019. Assimilation of satellite-based data for hydrological mapping of precipitation and direct runoff coefficient for the Lake Urmia Basin in Iran. Water 11, 1624.

Alam, K., Trautmann, T., Blaschke, T., 2011. Aerosol optical properties and radiative forcing over mega-city Karachi. Atmos. Res. 101, 773–782.

Alborzi, A., Mirchi, A., Moftakhari, H., Mallakpour, I., Alian, S., Nazemi, A., Hassanzadeh, E., Mazdiyasni, O., Ashraf, S., Madani, K., others, 2018. Climate-informed environmental inflows to revive a drying lake facing meteorological and anthropogenic droughts. Environ. Res. Lett. 13, 84010.

Ashouri, H., Hsu, K.-L., Sorooshian, S., Braithwaite, D.K., Knapp, K.R., Cecil, L.D., Nelson, B.R., Prat, O.P., 2015. PERSIANN-CDR: Daily Precipitation Climate Data Record from Multisatellite Observations for Hydrological and Climate Studies. Bull. Am. Meteorol. Soc. 96, 69–83. https://doi.org/10.1175/BAMS-D-13-00068.1

Bagchi, A., Paul, J.A., 2018. Youth unemployment and terrorism in the MENAP (Middle East, North Africa, Afghanistan, and Pakistan) region. Socioecon. Plann. Sci. 64, 9–20. https://doi.org/10.1016/j.seps.2017.12.003

Boschetti, M., Nutini, F., Manfron, G., Brivio, P.A., Nelson, A., 2014. Comparative analysis of normalised difference spectral indices derived from MODIS for detecting surface water in flooded rice cropping systems. PLoS One 9, e88741.

Chaudhari, S., Felfelani, F., Shin, S., Pokhrel, Y., 2018. Climate and anthropogenic contributions to the desiccation of the second largest saline lake in the twentieth century. J. Hydrol. 560, 342–353. https://doi.org/10.1016/j.jhydrol.2018.03.034

Chipman, J.W., Lillesand, T.M., 2007. Satellite-based assessment of the dynamics of new lakes in southern Egypt. Int. J. Remote Sens. 28, 4365–4379. https://doi.org/10.1080/01431160701241787

Dehgan, A., Palmer-Moloney, L.J., Mirzaee, M., 2014. Water security and scarcity: Potential destabilization in western Afghanistan and Iranian Sistan and Baluchestan due to transboundary water conflicts. Water and post-conflict peacebuilding 305.

Ehsani, M.R., Arevalo, J., Risanto, C.B., Javadian, M., Devine, C.J., Arabzadeh, A., Venegas-quiñones, H.L., Paige, A., Oro, D., Behrangi, A., 2020. Hydroclimatological and Vegetation Variabilities 1–18.

Farahmand, A., AghaKouchak, A., 2015. A generalized framework for deriving nonparametric standardized drought indicators. Adv. Water Resour. 76, 140–145.

Gorelick, N., Hancher, M., Dixon, M., Ilyushchenko, S., Thau, D., Moore, R., 2017. Google Earth Engine: Planetary-scale geospatial analysis for everyone. Remote Sens. Environ.

Goudie, A.S., Middleton, N.J., 2006. Desert dust in the global system. Springer Science & Business Media.

Goudie, A.S., Middleton, N.J., 2000. Dust storms in south west Asia. Acta Univ. Carolinae, Suppl. 7383.

Haghighi, A.T., Kløve, B., 2015. A sensitivity analysis of lake water level response to changes in climate and river regimes. Limnologica 51, 118–130.

Haghighi, A.T., Zaki, N.A., Rossi, P.M., Noori, R., Hekmatzadeh, A.A., Saremi, H., Kløve, B., 2020. Unsustainability syndrome-from meteorological to agricultural drought in arid and semi-arid regions. Water (Switzerland) 12. https://doi.org/10.3390/w12030838

Hamoon International Wetland Research Institute of Zabol University (HIWRI), 2017. Investigation of water requirement for Hamoon International Wetland in different water scenarios.

Hao, Z., AghaKouchak, A., Nakhjiri, N., Farahmand, A., 2014. Global integrated drought monitoring and prediction system. Sci. data 1, 1–10.

Hossenzadeh, S.R., 1997. One hundred and twenty days winds of Sistan. Iran Iran. J Res Geogr. 46, 103–127.

Huffman, G., Adler, R., Bolvin, D., Gu, G., Nelkin, E., Bowman, K., Hong, Y., Stocker, E., Wolff, D., 2007. The TRMM multi-satellite precipitation analysis: Quasi-global, multi-year, combined sensor precipitation estimates at fine scales. J. Hydrometeorol. 8, 28–55.

ICANA, 2015. 25% migration of Sistan people due to drought [WWW Document]. URL khabaronline.ir/news/587938 (accessed 8.25.20).

Iran Ministry of Enegry (MoE), 2013. Update of Sistan River studies (hydrological report).

Iranian Consultative Assembly News Aagency (ICANA), 2012. “Hamoon” is the artery of Sistan [WWW Document]. URL https://www.icana.ir/Fa/News/248571/%22هامون%22شاهرگ-سیستان--است (accessed 8.25.20).

Irannezhad, M., Haghighi, A.T., Chen, D., Kløve, B., 2015. Variability in dryness and wetness in central Finland and the role of teleconnection patterns. Theor. Appl. Climatol. 122, 471–486.

Khazaei, B., Khatami, S., Alemohammad, S.H., Rashidi, L., Wu, C., Madani, K., Kalantari, Z., Destouni, G., Aghakouchak, A., 2019. Climatic or regionally induced by humans? Tracing hydro-climatic and land-use changes to better understand the Lake Urmia tragedy. J. Hydrol. 569, 203–217.

Kottek, M., Grieser, J., Beck, C., Rudolf, B., Rubel, F., 2006. World map of the Köppen-Geiger climate classification updated. Meteorol. Zeitschrift 15, 259–263. https://doi.org/10.1127/0941-2948/2006/0130

Lehner, B., Liermann, C.R., Revenga, C., Vörösmarty, C., Fekete, B., Crouzet, P., Döll, P., Endejan, M., Frenken, K., Magome, J., others, 2011. High-resolution mapping of the world’s reservoirs and dams for sustainable river-flow management. Front. Ecol. Environ. 9, 494–502.

McKee, T.B., 1995. Drought monitoring with multiple time scales, in: Proceedings of 9th Conference on Applied Climatology, Boston, 1995.

Meteorological Department of Sistan and Baluchestan, 2020. 120-day wind speed [WWW Document]. URL https://sbmet.ir/ (accessed 6.3.21).

Mianabadi, H., Alioghli, S., Morid, S., 2021. Quantitative evaluation of ‘ No-harm ’ rule in international transboundary water law in the Helmand River basin. J. Hydrol. 599, 126368. https://doi.org/10.1016/j.jhydrol.2021.126368

Micklin, P.P., 1988. Desiccation of the Aral Sea: a water management disaster in the Soviet Union. Science (80-.). 241, 1170–1176.

Milly, P.C.D., Dunne, K.A., 2016. Potential evapotranspiration and continental drying. Nat. Clim. Chang. 6, 946–949.

Ministry of Cooperatives Labour and Social Welfare Iran, 2017. Employment status of Sistan and Baluchestan province.

Ministry of Energy (MoE), 2015. Report on water resources and consumption of Sistan and Baluchestan province.

Ministry of Energy (MoE), 2014. Studies of the second phase of water supply in Sistan plain. Tehran.

Miri, A., Ahmadi, H., Ghanbari, A., Moghaddamnia, A., 2007. Dust storms impacts on air pollution and public health under hot and dry climate. Int J Energy Env. 2, 101–105.

Ouma, Y.O., Tateishi, R., 2006. A water index for rapid mapping of shoreline changes of five East African Rift Valley lakes: an empirical analysis using Landsat TM and ETM+ data. Int. J. Remote Sens. 27, 3153–3181. https://doi.org/10.1080/01431160500309934

Pekel, J.F., Cottam, A., Gorelick, N., Belward, A.S., 2016. High-resolution mapping of global surface water and its long-term changes. Nature 540, 418–422. https://doi.org/10.1038/nature20584

Rahimi, R., Tavakol-Davani, H., Graves, C., Gomez, A., Valipour, M.F., 2020. Compound inundation impacts of coastal climate change: Sea-level rise, groundwater rise, and coastal precipitation. Water (Switzerland) 12, 1–16. https://doi.org/10.3390/w12102776

Rashki, A., Kaskaoutis, D.G., Goudie, A.S., Kahn, R.A., 2013. Dryness of ephemeral lakes and consequences for dust activity: The case of the Hamoun drainage basin, Southeastern Iran. Sci. Total Environ. 463–464, 552–564. https://doi.org/10.1016/j.scitotenv.2013.06.045

Rashki, A., Kaskaoutis, D.G., Rautenbach, C.J. d. W., Eriksson, P.G., Qiang, M., Gupta, P., 2012. Dust storms and their horizontal dust loading in the Sistan region, Iran. Aeolian Res. 5, 51–62. https://doi.org/10.1016/j.aeolia.2011.12.001

Rokni, K., Ahmad, A., Selamat, A., Hazini, S., 2014. Water Feature Extraction and Change Detection Using Multitemporal Landsat Imagery 4173–4189.

https://doi.org/10.3390/rs6054173

Rouse Jr, J.W., 1973. Monitoring the vernal advancement and retrogradation (green wave effect) of natural vegetation.

Schneider, U., Becker, A., Finger, P., Meyer-Christoffer, A., Rudolf, B., Ziese, M., 2011. Monthly land-surface precipitation from rain-gauges built on GTS-based and historic data. Glob. Precip. Clim. Cent.(GPCC), Dtsch. Wetterdienst, doi 10.

Shukla, S., Wood, A.W., 2008. Use of a standardized runoff index for characterizing hydrologic drought. Geophys. Res. Lett. 35.

Statistical Center of Iran, 2016. Results of the general population and housing census in 2016 [WWW Document]. URL https://www.amar.org.ir/english (accessed 11.26.20).

Tadono, T., Nagai, H., Ishida, H., Oda, F., Naito, S., Minakawa, K., Iwamoto, H., 2016. Generation of the 30 M-mesh global digital surface model by ALOS PRISM. Int. Arch. Photogramm. Remote Sens. Spat. Inf. Sci. 41.

The Convention on Wetlands, 1975. Ramsar Sites Information Service [WWW Document]. URL https://rsis.ramsar.org/ (accessed 1.1.20).

Thom, H.C.S., 1966. Some methods of climatological analysis. WMO Tech. Note81.

Torabi Haghighi, A., Fazel, N., Hekmatzadeh, A.A., Klöve, B., 2018. Analysis of Effective Environmental Flow Release Strategies for Lake Urmia Restoration. Water Resour. Manag. 32, 3595–3609. https://doi.org/10.1007/s11269-018-2008-3

Torabi Haghighi, A., Sadegh, M., Behrooz-Koohenjani, S., Hekmatzadeh, A.A., Karimi, A.,

Kløve, B., 2020. The mirage water concept and an index-based approach to quantify causes of hydrological changes in semi-arid regions. Hydrol. Sci. J. 65, 311–324.

WHO, 2016. Global Health Observatory data repository [WWW Document]. World Heal. Organ. URL https://apps.who.int/gho/data/view.main.AMBIENTCITY2016?lang=en (accessed 11.8.20).

Williams-Sether, T., 2008. Streamflow characteristics of streams in the Helmand Basin, Afghanistan. US Department of the Interior, US Geological Survey.

Zaki, N.A., Haghighi, A.T., Rossi, P.M., Tourian, M.J., Bakhshaee, A., Kløve, B., 2020. Evaluating impacts of irrigation and drought on river, groundwater and a terminal Wetland in the Zayanderud Basin, Iran. Water (Switzerland) 12. https://doi.org/10.3390/W12051302

Zaki, N.A., Haghighi, A.T., Rossi, P.M., Xenarios, S., Kløve, B., 2018. An index-based approach to assess thewater availability for irrigated agriculture in sub-Saharan Africa. Water (Switzerland) 10. https://doi.org/10.3390/w10070896